The Department of Energy's Atmospheric Radiation Measurement (ARM) Unmanned Aerospace Vehicle (UAV) Program

G. L. Stephens,[a] R. G. Ellingson,[b] J. Vitko Jr.,[c] W. Bolton,[c] T. P. Tooman,[c] F. P. J. Valero,[d] P. Minnis,[e] P. Pilewskie,[f] G. S. Phipps,[g] S. Sekelsky,[h] J. R. Carswell,[h] S. D. Miller,[a] A. Benedetti,[a] R. B. McCoy,[a] R. F. McCoy Jr.,[a] A. Lederbuhr,[i] R. Bambha[j]

ABSTRACT

The U.S. Department of Energy has established an unmanned aerospace vehicle (UAV) measurement program. The purpose of this paper is to describe the evolution of the program since its inception, review the progress of the program, summarize the measurement capabilities developed under the program, illustrate key results from the various UAV campaigns carried out to date, and provide a sense of the future direction of the program. The Atmospheric Radiation Measurement (ARM)–UAV program has demonstrated how measurements from unmanned aircraft platforms operating under the various constraints imposed by different science experiments can contribute to our understanding of cloud and radiative processes. The program was first introduced in 1991 and has evolved in the form of four phases of activity each culminating in one or more flight campaigns. A total of 8 flight campaigns produced over 140 h of science flights using three different UAV platforms. The UAV platforms and their capabilities are described as are the various phases of the program development. Examples of data collected from various campaigns highlight the powerful nature of the observing system developed under the auspices of the ARM–UAV program and confirm the viability of the UAV platform for the kinds of research of interest to ARM and the clouds and radiation community as a whole. The specific examples include applications of the data in the study of radiative transfer through clouds, the evaluation of cloud parameterizations, and the development and evaluation of cloud remote sensing methods. A number of notable and novel achievements of the program are also highlighted.

1. Introduction

The potential of the unmanned aerospace vehicle (UAV) as a platform for carrying instruments to observe the atmosphere and underlying surface has been contemplated for some time. Interest in these platforms continues to be stimulated in part by the availability of military surveillance aircraft to the civilian research community and in part by the rapidly expanding technologies that provide a more reliable operation of these aircraft through improved communication, navigation, and data telemetry systems. The potential for operation at high altitudes (up to and above 20 km) for long periods of time (in excess of 24 h) and at low airspeed, together with the expansion of available payloads in recent years, add to the overall desirability of UAVs as observing platforms for atmospheric and remote sensing research.

[a]Department of Atmospheric Sciences, Colorado State University, Fort Collins, Colorado.
[b]Department of Meteorology, University of Maryland, College Park, Maryland.
[c]Sandia National Laboratories, Livermore, California.
[d]Scripps Institution of Oceanography, San Diego, California.
[e]Atmospheric Science Division, NASA Langley Research Center, Hampton, Virginia.
[f]NASA Ames Research Center, Sunnyvale, California.
[g]Sandia National Laboratories, Albuquerque, New Mexico.
[h]University of Massachusetts, Amherst, Massachusetts.
[i]Lawrence Livermore National Laboratory, Livermore, California.
[j]Crocker Nuclear Laboratory, University of California, Davis, Davis, California.
Corresponding author address: Graeme Stephens, Department of Atmospheric Science, Colorado State University, Fort Collins, CO 80523-1371.
E-mail: stephens@langley.atmos.colostate.edu
In final form 14 July 2000

Although the potential of UAVs has long been appreciated, demonstration of the advantages of these platforms over manned aircraft under actual operating conditions encountered in complex scientific experiments is generally lacking. This apparent lack of demonstration exists despite the ongoing development of various autonomous aircraft that offer a range of altitude, duration, and payload-carrying capabilities. For example, Aurora Flight Services continues to develop and test the Perseus line of UAVs (Langford 1990) and have introduced the Theseus concept UAV with more payload and altitude capability than that of the Perseus. Scientific experiments with these aircraft exist only as concepts at this time (e.g., Albritton et al. 1991; Langford 1990). Holland et al. (1992) describe the Aerosonde concept that is a small, inexpensive, and reusable aircraft capable of lifting a few kilogram payload to about 5 km. Although test flights with this UAV indicate significant potential for sounding the lower atmosphere, only very basic and simple payloads with elementary data systems have been flown to date. Military interest in extremely long endurance, high-altitude UAVs led to the development of the Boeing *Condor* in the early 1980s. This aircraft used two, dual-stage turbo-charged, piston engines driving large diameter propellers to achieve multiday endurance at altitudes as high as 20 km (67 000 ft) with a payload weight on the order of 1000 kg (2200 lb). Although the *Condor* offered extremely impressive performance, its size, complexity, and cost made it ill suited for climate research, as contemplated by UAV programs mentioned below. However, the use of lightweight, aerodynamically efficient composite airframe construction and multistage turbo-charged piston engines, like that developed for *Condor*, with advances in low-cost, powerful digital processing capabilities led to the class of high-altitude, long-endurance UAVs offered by Aurora Flight Services and General Atomics-Aeronautical Systems and others. These relatively low-cost UAVs provided a capability well suited to aircraft-based research programs.

Three UAV-based research flight programs have been established by different agencies within the United States connected in part with the above-mentioned ongoing development of UAV platforms. The evolution of these programs has not been entirely independent of one another. Both the National Aeronautics and Space Administration (NASA) and the Office of Naval Research (ONR) have put in place programs dedicated to promoting the use of UAVs as a platform for environmental research. NASA's Environmental Research Aircraft and Sensor Technology program (ERAST; available online at http://www.dfrc.nasa.gov/Projects/Erast) is currently developing a family of high-altitude, long-endurance, and relatively low operational cost UAVs for environmental research. The ONR, in conjunction with the Naval Postgraduate School, California Institute of Technology, and Princeton University, has developed the Center for Interdisciplinary Remotely Piloted Aircraft Studies (CIRPAS; see Bluth et al. 1996; available online at http://web.nps.navy.mil/~cirpas/) to support atmospheric and oceanographic research and technology development. CIRPAS proposes to operate three types of UAVs including the above-mentioned Aerosonde and the General Atomics Aeronautical Systems Altus aircraft in partnership with the Department of Energy (DOE) Atmospheric Radiation Measurement (ARM) Program.

The U.S. DOE through the ARM program is the third agency to establish a UAV-based measurement program (available online at http://armuav.atmos.colostate.edu). This program, hereafter referred to as the ARM–UAV program, was originally developed as part of the Atmospheric Remote Sensing and Assessment Program (ARSAP). The ARSAP is a joint program between the Department of Defense (DoD) and DOE developed as part of the global environmental change thrust of the Strategic Environmental Research and Development Program (SERDP). ARSAP was funded from FY91 through FY95 to develop improved measurements for studying the earth's atmosphere. The DoD focused on the stratosphere and mesosphere whereas the DOE's interests were directed to the troposphere.

The ARM–UAV program has evolved considerably since the original period of SERDP funding. This program has been based on the availability of existing UAVs that were originally developed for military surveillance purposes. The ARM–UAV program has integrated multiple payloads and provided 540 flight hours of quality research data obtained from a number of field campaigns and as a result of this activity has convincingly demonstrated the viability of UAVs in atmospheric research. The purpose of this paper is to describe the ARM–UAV program and its evolution since its inception, assess the progress of the program, summarize the measurement capabilities developed under the program, illustrate key results from the various UAV campaigns carried out to date and a vision for the future direction of the program.

The paper begins with an overview of the research and technical thrusts of the ARM–UAV program. This

is followed in section 3 with a summary of the aircraft platforms operated during the various campaigns that have been carried out since 1993. Section 4 overviews payload elements specifically developed under the program, section 5 describes the data systems and data protocols established for the measurement campaigns, and section 6 presents selected highlights of results obtained from the measurements carried out to date. The paper concludes with a summary and a review of the progress of the ARM–UAV program.

2. The ARM–UAV concept

The ARSAP program sought to develop improved measurements that could contribute toward an enhanced understanding of the earth's atmosphere and its response to global change. The program sought to exploit and apply unique DoD and DOE technologies as a way of contributing to this programmatic goal. The ARM–UAV program, in turn, contributes to this goal through the pursuit of the following scientific and technological objectives.

1) The ARM–UAV program seeks to incorporate new measurement technologies on UAV platforms providing observations that contribute meaningfully to our understanding of cloud and radiation interactions. The program has not only supported the development of new instruments and data systems but has also supported the adaptation of other instruments to the UAV environment.
2) The program also seeks to demonstrate the capabilities of selected UAV platforms operating under the varying constraints established by different science experiment scenarios. This has involved, among others, the development of techniques to formation fly UAVs and provide real-time data down linked to the instrument mentor located at a remote operating center.

A systematic approach involving four phases of activities was developed to meet these objectives while taking maximum advantage of increasing instrument and UAV capabilities that evolved throughout the period of the 1990s. The specific goals of the first three phases of the program have been achieved through a series of measurement campaigns summarized in Table 1. In all campaigns, since phase I, measurements from manned aircraft have either augmented the UAV measurements or have substituted for the latter when the UAV platforms were unavailable for any given campaign. The use of manned aircraft as opposed to UAV aircraft is also indicated in Table 1.

Phase I: Phase I began in 1993 and sought to demonstrate the viability of making atmospheric profile measurements of clear-sky radiative fluxes and related atmospheric variables using a single UAV platform, in this case the Gnat-750 UAV built by General Atomics Aeronautical Systems, Inc. The activity of phase I included two flight series. The first was a series of engineering test flights conducted in restricted air space at Edwards Air Force base in November 1993. The second campaign operated from the Blackwell Tonkawa Airport approximately 10 nautical miles from the ARM Southern Great Plains (SGP; Stokes and Schwartz 1994) site during the spring of 1994 (hereafter referred to as S94). The payload consisted of seven instruments, a pair of matched broadband solar and infrared hemispheric radiometers, the total diffuse direct radiometer (TDDR; e.g., Valero et al. 1982) mounted in the zenith position measuring downwelling radiation in seven solar bands, the Spectrally Scanning Polarimeter (SSP; Stephens et al. 2000), and a suite of instruments measuring temperature and dewpoint. Clear-sky profiles of temperature, water vapor, and short- and longwave fluxes were thus obtained from the flights conducted under this campaign and analyses of these measurements are summarized by Valero et al. (1996).

Phase II: The principal technical goal of phase II was to fly the UAV platform in formation with a second (manned) aircraft and to connect the observations from both aircraft to surface and satellite observations. This activity began with the fall 1995 (F95) campaign (also referred to as ARESE; e.g., Valero et al. 1997). Since the UAV was unavailable for this campaign, two manned aircraft were equipped with radiometers and flew a tightly stacked formation with one aircraft above the other to provide solar flux measurements above and below the cloud. The science payload included two additional solar radiometers covering the spectral range 0.7–3.0 μm in lieu of the infrared radiometer, the addition of a second TDDR mounted in the nadir position, and the cloud detection lidar (CDL). A number of papers report on the results of the ARESE campaign (e.g., Valero et al. 1997; Li et al. 1999) including multiple aircraft observing system simulation studies (Marshak et al. 1997).

Phase II continued with the spring of 1996 (S96) campaign by repeating the earlier two manned aircraft experiment. In this campaign, the Egrett also flew the

TABLE 1. Summary of the ARM–UAV Program experimental campaigns. Four of the eight campaigns to date deployed UAVs that are identified in italics. Refer to Table 3 for payload description.

Campaign date	Development phase (refer text)	Platforms (UAVs in italics)	No. of flights and science flight h[c]	Highlights
Nov 1993	Phase I	*Gnat-750*	1 flight 3 h	
Apr 1994 (S94)	Phase I	*Gnat-750*, DHC-6 Twin Otter as chase	8 flights 22 h	First science flights in unrestricted airspace. First radiation flux profiles from a UAV up to 7 km
Fall 1995 (F95)	Phase II	Egrett and Otter	10 flights 52 h	Coordination of two aircraft above and below cloud. ARESE experiment with a few days of solid layered clouds. First flight of the CDL.
Spring 1996 (S96)	Phase II	Egrett and Otter	7 flights 70 h	Two aircraft flights repeated—clouds were largely broken, some cirrus. First flight of the MPIR and frost point hygrometer
Fall 1996 (F96)	Phase III	*Altus* and Otter	5 flights 60 h	First flight of the Altus UAV—coordinated with manned aircraft flights (29 Sep). Long duration on station for 24 h (Fig. 1). First unescorted science flight of UAV in civilian airspace.
Fall 1997 (F97)	Phase III	*Altus II* and Otter	5 flights 19 h	First flight of the Altus II, mostly clear-sky flights
Spring 1999[a] (S99)	Phase III	*Altus II* and Otter	6 flights 37 h	Coordinated measurements from UAV and manned aircraft. First scientific operation of the UAV at scientific operation of the UAV at 55 000 ft
Summer 1999[b] (Su99)	Phase IV	Otter and CIRPAS Otter	10 flights 35 h	Coordinate flight of UAV payload on manned aircraft with in situ measurements. First flight of UAV cloud radar.

[a]In collaboration with NASAs ERAST and Earth System Science Cloud, Aerosol, and Radiation program
[b]In collaboration with NASA Earth System Science Cloud, Aerosol, and Radiation program and ONR
[c]Flight numbers and hours to the first mentioned aircraft listed in the third column

newly developed frost point hygrometer and the Multispectral Pushbroom Imaging Radiometer (MPIR) instrument (discussed in more detail below). In total, seven flights were conducted in conditions ranging from clear skies to overcast stratus over a 3-week period. Fluxes measured above different cloud conditions provided a source of information to evaluate the vicarious calibration of the satellite radiance-to-flux algorithms (e.g., Mayor et al. 1998). This campaign also provided measurements above cirrus clouds in con-

junction with the Subsonic Aircraft contrail and Cloud Effects Special study (Toon and Miake-Lye 1998).

Phase II concluded with the fall of 1996 (F96) campaign with the first scientific flights of the General Atomics Altus UAV. The technical goals of Phase II were thus achieved with the completion of this campaign. The payload carried by the Altus included all instruments flown previously on the Egrett for the S96 campaign. Flights were mainly conducted in clear-sky conditions and were coordinated carefully with the Twin Otter using procedures developed for ARESE. The experiments yielded clear-sky profiles of radiative fluxes and water vapor. The flight of 4/5 October 1996 was noteworthy setting a record for the longest continuous measurements of the diurnal cycle of radiative fluxes over the SGP from a UAV as shown in Fig. 1. For this flight the Altus was maintained on station at approximately 6 km for over 24 h.

Phase III: This phase of the program extended the operational altitude of the UAV upward to acquire science data at altitudes up to approximately 16 km. Phase III began with the fall of 1997 (F97) campaign using the Altus as previously used during F96. The first science measurements in this campaign were obtained on 26 September as part of a dual-aircraft measurement strategy. For this particular campaign, the Altus operated at or below 11 km. Figure 2 below is a sample of the water vapor profile measured with the frost point hygrometer flown on both the Altus and Twin Otter in clear skies on 26 September. These profiles are contrasted in this figure against radiosonde water vapor profile data obtained some two hours prior to the flights as part of a water vapor measurement intensive observing period that ran concurrently with the F97 campaign.

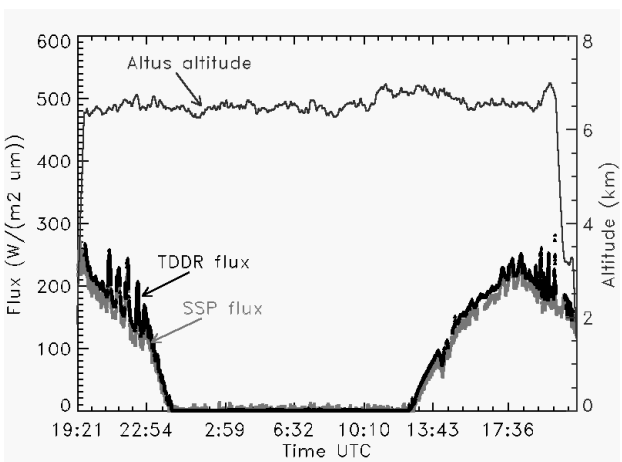

FIG. 1. Time series of the Altus altitude for the record-setting flight conducted on 4/5 Oct 1996 indicating an on station time of 24 h and 46 min. The lower panel provides time series of the measured solar fluxes at 0.86 μm reflected from the atmosphere and surface below the Altus as measured during flight by the TDDR and SSP.

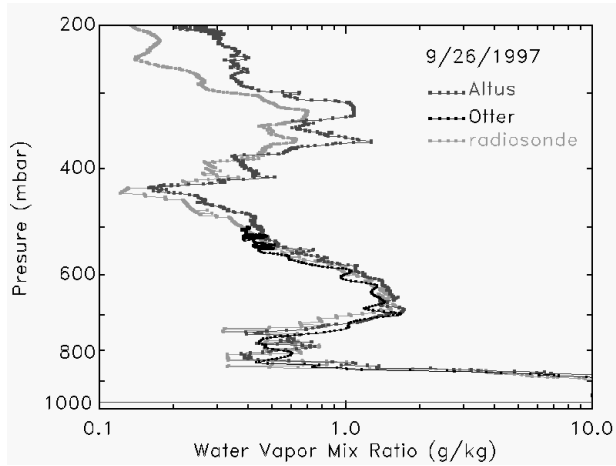

FIG. 2. Profiles of water vapor mixing ratio measured by the frost point hygrometer flown on both the Altus and Twin Otter over the SGP site during the F97 campaign. The aircraft measured profiles are contrasted with the profile obtained from radiosonde launched over CART site 2 h prior to the aircraft descent.

Phase III continued with the spring of 1999 (S99) campaign that operated from the Pacific Missile Range Facility, Kauai, Hawaii (in contrast to all previous campaigns based out of the Blackwell-Tonkawa Airport and flown over the SGP site). This experiment was designed as a two-aircraft cirrus cloud experiment and deployed the Altus II for the first time. During the S99 campaign the Altus II operated for 16.5 h at or above 15.24 km (50 000 ft) and 1.75 h above 16.75 km (55 000 ft) where it generally flew above all cirrus and in tight formation with the Twin Otter that flew below cloud base. The Altus II provided measurements of spectral and broadband radiative fluxes, spectral radiances, and lidar backscattering properties of tropical and subtropical cirrus. The Twin Otter provided similar radiometric measurements below the cloud as well as radar reflectivity measurements obtained using the NASA Jet Propulsion Laboratory/University of Massachusetts' 94-GHz airborne cloud radar (Sadowy et al. 1997).

Phase IV: The ARM–UAV program has now entered its fourth phase of development. Under this phase, the program seeks to accomplish the following.

1) Provide measurements from a UAV at an altitude up to 20 km being more typical of the altitudes of

TABLE 2. Summary of the two manned and three UAV ARM–UAV Aircraft Characteristics (UAV airframes are identified in italics).

Aircraft	Aircraft type	Altitude km (ft)	Payload kg (lbs)	Endurance h	Total science flight h
Gnat 750-45	UAV; single engine/prop;	7.6 (25 000)	70 (150)	40	25
Egrett	Piloted, single engine turbine/prop;	13.7 (45 000)	450 (1000)	10+	122
Twin Otter	Piloted, twin engine turbine/prop	7.6 (25 000)	2045 (4500)	4+	278
Altus	UAV, single engine/prop, 4-cylinder; single-stage turbocharged	12.2 (40 000)	150 (330)	24+	116 for Altus and Altus II
Altus II	UAV, single engine/prop, 4-cylinder, two-stage turbocharged	19.8 (65 000)	150 (330)	12+	

the tropical tropopause in regions of deep convection. This altitude capability is needed for observing upper-tropospheric clouds and for profiling upper-tropospheric water vapor in these regions.

2) Coordinate flights of two UAVs, one observing clouds from above (or below) with the radiometric and remote sensing sensors already developed under the activities of Phases I–III and a second UAV providing matched measurements of microphysical properties within the cloud.

Phase IV began with an experiment carried out over the Pacific Ocean off the coast of Monterey, California, in July 1999. This experiment, jointly coordinated with both NASA and ONR support, primarily involved two Twin Otter (manned) aircraft flying coordinated patterns as well as occasional coordinated flights with the NASA ER2. The experiment yielded measurements of clouds observed with the UAV payload with the addition of the NASA cloud radar aboard one Twin Otter and the simultaneous measurements of the microphysics of the clouds obtained with the second CIRPAS Twin Otter aircraft. This experiment also provided the opportunity for the maiden flight of the ARM–UAV cloud radar that is planned to participate in future UAV campaigns. Planning for these future Phase IV campaigns is currently in progress.

3. Aircraft platforms and overview of platform achievements

The eight campaigns summarized in Table 1 deployed five different aircraft platforms, two manned aircraft (Egrett and Otter) and three UAV platforms, namely the Gnat-750, the Altus and the Altus II. The Altus and Altus II provided the majority of the UAV flight hours for the program. The Altus shares much of the design philosophy and many systems with the Predator UAV, developed for the U.S. military as a reconnaissance platform and used extensively in that role in recent years. Altus has a composite airframe, approximately a 16.8-m (55 ft) wingspan, a four-cylinder air/liquid cooled engine and pusher propeller. When equipped with a single stage of turbo charging, the Altus is capable of operating at altitudes of approximately 11 km (37 000 ft) while carrying a payload in excess of 150 kg. The Altus II carries the same payload but the dual-stage turbo charging lifts that airframe and payload above 16 km.

Table 2 summarizes the basic capabilities of each of the five aircraft platforms and Fig. 3a provides a view of the three UAVs flown and an expanded view of the payload flow on the Altus (Fig. 3b). In addition to the valuable science data collected, the ARM–UAV program recorded a number of notable programmatic achievements.

(a)

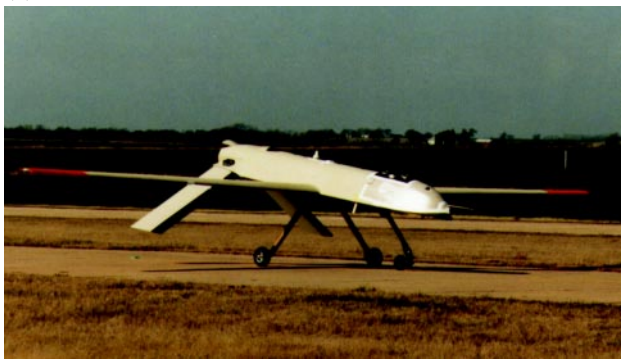

(b)

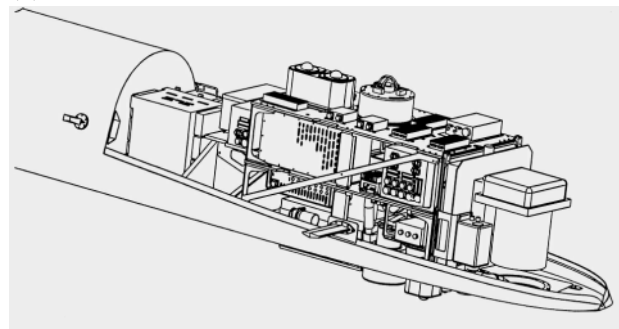

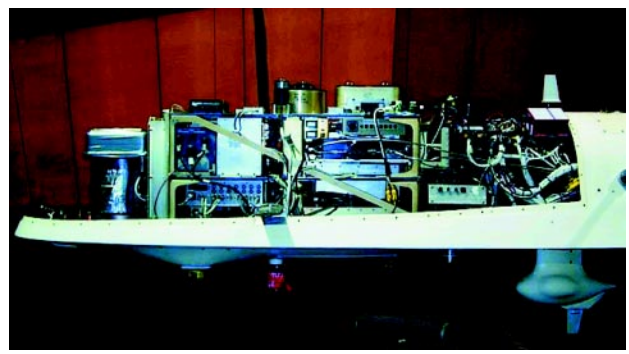

FIG. 3. (a) The three UAV platforms: Gnat, Altus, and Altus II employed under the ARM–UAV program in different campaigns. (b) Extended views of the payload configured on Altus.

1) The ARM–UAV program conducted the first science flights using a UAV to profile the atmosphere up to 7 km during the S94 campaign. The data were telemetered from the Gnat to the ground using the system specifically developed for the program and discussed below. Since the flights of S94 were the first UAV flights in nonrestricted airspace, the UAV had to be accompanied with a chase aircraft (the DHC-6 Twin Otter) that was also used as an additional platform for science measurements in later campaigns.
2) The first unescorted flights of a UAV above 5.6 km (18 500 ft, and referred to as Class "A" airspace) on 29 September 1996. The chase plane restrictions were lifted for subsequent campaigns for flights in Class A airspace. Since the service ceiling of the Altus is above 11 km, the chase plane was only required to escort the UAV to 6 km making it possible to fly the UAV unescorted above that altitude.
3) A commercial GPS-based navigation system was adapted to meet the needs of the ARM–UAV program and was included with all payloads. With this system, the horizontal position of one aircraft relative to another could be controlled within 100 m with aircraft separated by 12 km or more in altitude (Fig. 4a). This capability proved to be important for many of the science goals of individual experiments and was employed in the F97 campaign when the first measurements from a coordinated flight of a UAV with a second (manned) aircraft were obtained. A second feature of the UAV platforms used is the high level of stability of the platform that could be maintained with wings level to a high degree of accuracy indicated by the pitch and roll information recorded during flight as shown in Fig. 4b.

(a)

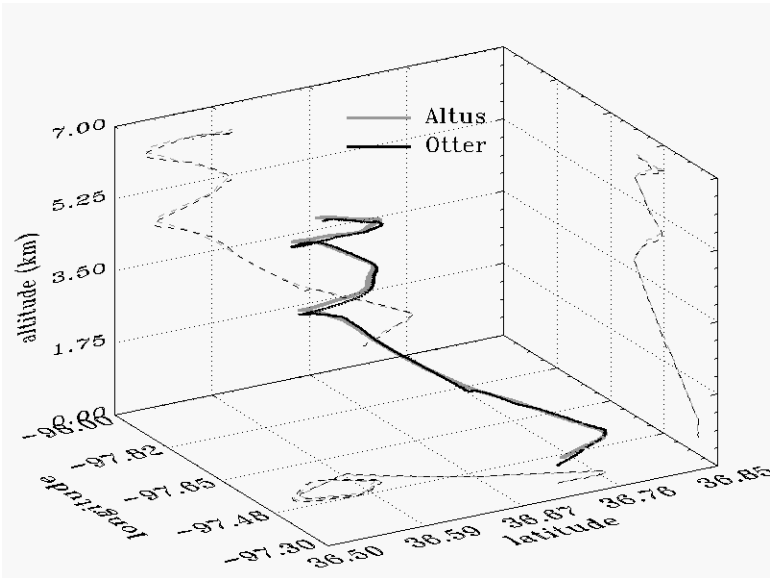

(b)

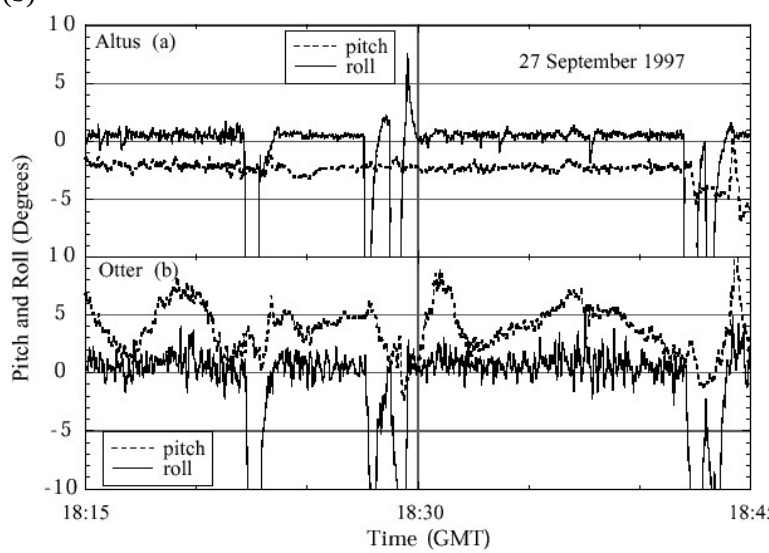

FIG. 4. (a) An example of the formation flying between the Altus UAV and the Twin Otter for the flight of 4 Oct 1990. (b) Comparison of aircraft pitch and roll from the (a) Altus and (b) Otter from a wings level, side-by-side radiometer intercomparison flight on 27 Sep 1997 at a flight level of about 4 km. Large variations of the roll indicate turns. The stable characteristics of the UAV platform are illustrated by the very small variation of the roll and pitch of the Altus relative to the manned Otter.

4) The F97 campaign also produced the record setting flight of 4/5 October 1996 in which the Altus set a new endurance record for airborne scientific study being on station at 6 km for 24 h and 46 min.
5) The S99 campaign provided the first extensive science measurements from a UAV flown above 16 km.

4. The ARM–UAV payload capabilities

The ARM–UAV payload has evolved considerably since the first engineering flights of 1993. Seven new UAV-compatible instruments have been developed under the program, five have flown in the eight campaigns and the other two sensors have not flown due to funding shortfalls. The instruments specifically developed are the CDL, Frost Point Hygrometer, Atmospheric Emitted Radiance Interferometer (mini-AERI), Hemispherical Optimized Net Radiometer (HONR), MPIR, the Compact Millimeter-wave Radar (UAV-CMR) and the SSP (Stephens et al. 2000). In addition to these instruments, the program has also supported the integration of existing instruments in the payload as well as a calibration facility at the Los Alamos National Laboratory (the appendix). Table 3 overviews key properties of the instruments flown on the different aircraft platforms and the lead organization in charge of the instrument, including calibration and data processing. The characteristics of four of the new instruments developed specifically for the UAV environment are also discussed in more detail below. Further details of the instruments can be found online at http://armuav.atmos.colostate.edu/armuav3.html.

A suite of instruments provided by Francisco Valero and his team originally located at NASA Ames Research Center and later at Scripps were also adapted to the UAV payload. This suite of radiometers is referred to as the Radiation Measurement System (RAMS) and includes a pair of matched shortwave broadband hemispherical radiometers mounted pointing to the zenith and to the nadir, measuring downwelling and upwelling solar radiation, respectively. A similar pair of shortwave flux radiometers limited to wavelengths longer than 0.68 μm when included as part of the RAMS and combined with broadband solar flux measurements provides a way of separating visible from near-infrared solar fluxes (e.g.,

TABLE 3. The ARM–UAV instruments.

Instrument	Status	Key instrument parameters	Lead organization
CDL	Flight unit and engineering model. First flight, F95 and flown in all subsequent campaigns	Weight 28 kg, Power 100W Wavelength 1.053 μm Pulse length 20 ns Repetition rate 5 kHz Output energy 48 μJ/pulse	Lawrence Livermore National Laboratory
AERI	Not flown		University of Wisconsin
HONR	Not flown		Los Alamos National Laboratory
MPIR	First flight, S96 Far infrared channels not included		Sandia National Laboratories
frost point and laser diode hygrometers	First Flight of the Frost point hygrometer, S96		Brookhaven National Laboratory
SSP	First flight, F94 and flown in all subsequent campaigns		Colorado State University
UAV-CMR	First flight, Monterey 1999	Power 110W Weight 30 kg Volume 1.5 ft^3 Pulse length 100 ns	University of Massachusetts
RAMS	Flown in all campaigns but with different configurations of radiometers (see text)		Scripps Institute of Oceanography
SSFR	First flight, S99		NASA, AMES

Valero et al. 1997). Similarly a pair of matched longwave broadband hemispherical radiometers to measure downwelling and upwelling thermal radiation are also part of the RAMS system as are a pair of TDDR that measured upwelling and downwelling radiation in seven solar bands from 0.38 to 1.6 μm.The TDDR has two external moving rings that periodically shade the radiation input port from direct solar radiation, allowing for the division of downwelling radiation into direct and diffuse fields. This division is important for the correction of downwelling shortwave broadband data for aircraft roll and pitch and for the determination of atmospheric aerosol loading.

The Solar Spectral Flux Radiometer (SSFR) developed by P. Pilewskie at NASA Ames has also been flown in two of the campaigns. The SSFR is a moderate resolution flux (irradiance) or intensity (radiance) spectrometer covering the wavelength range from

(a)

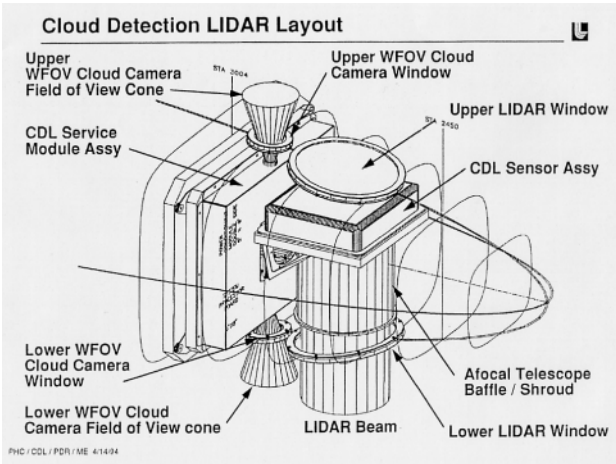

(b)

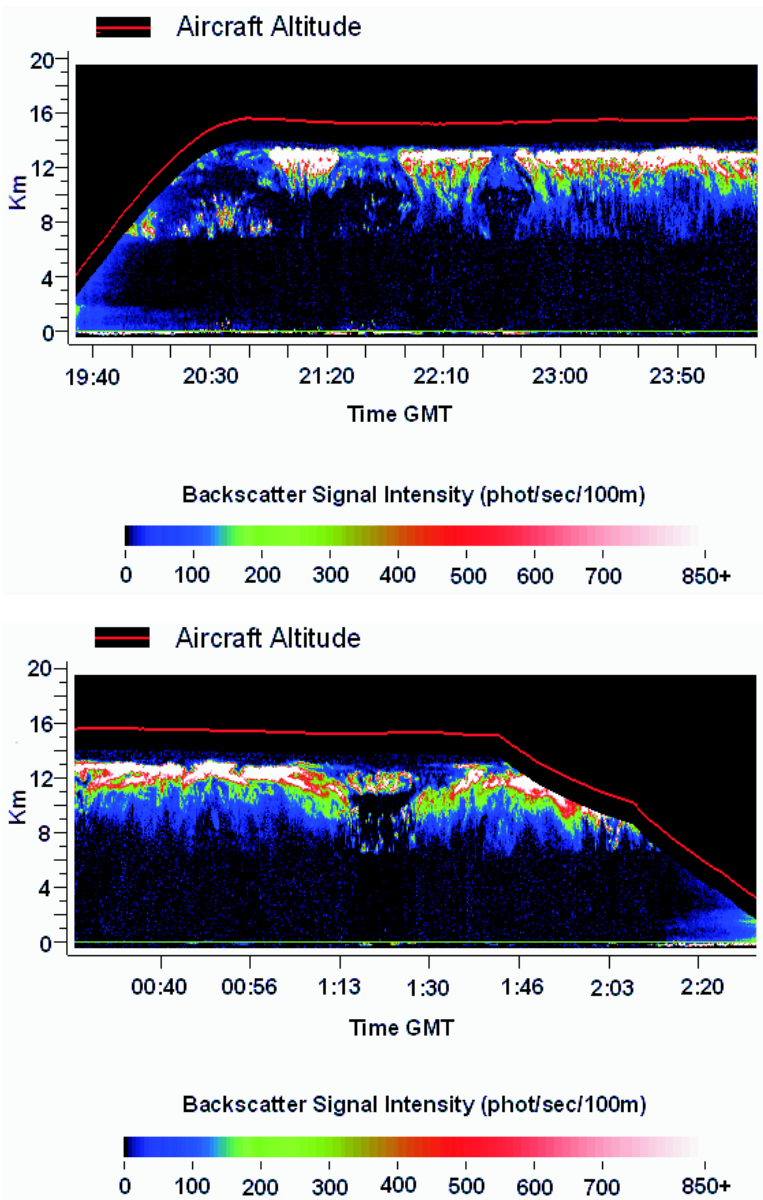

300 to 2200 nm. The estimated rms flux uncertainty is 3% to 5% for the SSFR spectral range between 300 to 2200 nm. SSFR rms *precision*, however, is far better, between 0.1% and 0.3% and plans are underway to improve the calibration procedure. Further details of the instrument and its applications can be found in Pilewskie et al. (1998).

a. The CDL instrument package

The CDL instrument package has flown in the S95, S96, F96, S97, and S99 campaigns. The CDL instrument package is composed of three instruments: the CDL built by Lawrence Livermore National Laboratory and two wide field-of-view cameras. The latter are charge coupled device cameras that are uncalibrated and used only to provide photographic documentation of the extent of cloud cover and some information on the type and variety of ground cover. One camera views nadir and the other views the zenith sky. Only one camera may be operational at a time.

The main sensor assembly of the CDL contains a laser diode-pumped Nd:YLF laser with an output wavelength of 1.053 μm and operating at 5-kHz repetition rate with Q-switched 20-ns long pulses of 48 μJ/pulse. The return time from a pulsed 1.053-μm laser gives the range to the target while the amplitude of the return signal provides information on the cloud and aerosol density or ground albedo. This system was developed to be a particularly compact and ruggedized, fully eye-safe, high-performance backscatter lidar. The CDL is designed to profile to a range of 20 km with a selectable range resolution to a minimum of 50 m. The lidar uses a common aperture 20-cm-diameter telescope to output the transmitter beam and receive the backscattered radiation. The system is made eye-safe through a novel approach of operating

FIG. 5. (a) A schematic of the CDL showing its location as part of the instrument payload in the nose of the airframe of the Altus. (b) Profiles of lidar backscatter from a thin cirrus layer as observed by the CDL plotted as a function of time (GMT) along the flight track of the Altus. The altitude of the UAV is also provided for reference.

with rapid but very low energy pulses expanded over the aperture of the telescope. The system is designed to autonomously provide a single measurement each second, which is an average of 5000 separate profiles to enhance the effective signal to noise. This provides profiles from much lower (eye-safe) energy per pulse output. The lidar can be rotated to perform cloud detection either above or below the aircraft.

Figure 5a shows a schematic of the instrument mounted in the nose of the airframe of the Altus and Fig. 5b provides an example of the data collected above a cirrus cloud layer observed by the CDL flying on the Altus II on 28 April during the S99 campaign. The data are the measured backscatter profiles along the flight track of the Altus II. The flight altitude of the UAV is also indicated for reference. The backscatter data indicates a layer of cirrus cloud between 10 and 12 km.

b. The MPIR

The MPIR is a radiometrically calibrated imaging device designed to measure simultaneously spectral radiances in the nine spectral bands or channels identified in Table 4. The images from the MPIR are created from the radiance data obtained from the linear detector arrays of the instrument that are swept along in the direction of the aircraft in a "push-broom" mode as shown in Fig. 6. The images constructed in this way extend 40° on each side of the aircraft with a horizontal resolution of 256 pixels except for channel one that has 512 pixels. At a flight level 8 km above the surface each pixel has a cross-track footprint of about 50 m at nadir (25 m for channel 1).

MPIR has nine interchangeable detector modules for each of the nine spectral channels. Each channel has its own coaligned optics, linear detector arrays, signal electronics, and digital signal processors to produce a serial, digital output of the image data. Although selection of alternate spectral bands would make MPIR adaptable to many remote sensing applications, its original nine bands were chosen to provide identification and characterization of cloud properties consistent with radiance data currently available from a number of sensors flown on both operational and experimental satellites, including the Moderate Resolution Imaging Spectrometer (King et al. 1992).

The four distinct types of detector arrays used in the MPIR modules are also indicated in Table 4. During the S96 test series, only the two Si and two InGaAs modules were installed and operational the

TABLE 4. MPIR channel assignments.

Channel	Bandwidth (μm)	Detector	Usage
1	0.62–067	Si	A,B,F,G,H,I
2	0.86–0.90	Si	A,F,G,H,I
3	1.36–1.39	InGaAs	C,D,I
4	1.58–1.64	InGaAs	A,B,F,G,I
5	2.11–2.22	InSb	A,B,F
6*	3.55–3.93	InSb	A,B,F,I
7*	6.54–6.99	HgCdTe	C
8*	8.40–8.70	HgCdTe	A,C,D,E,F,H
9*	10.3–11.3	HgCdTe	A,C,D,E,F,I

Usage key
A = cloud identification and amount
B = cloud thickness, particle size, phase
C = upper-tropospheric water vapor
D = cirrus detection
E = surface and cloud temperatures
F = surface properties
G = vegetation
H = aerosol detection
I = satellite calibration

*channels not yet flown

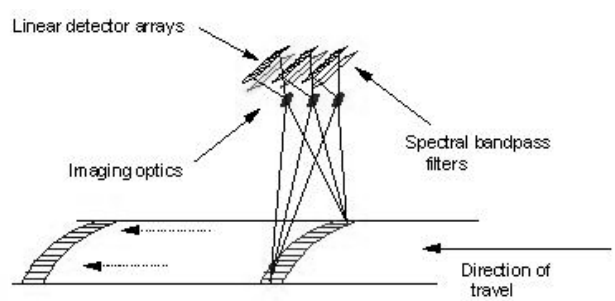

FIG. 6. The push-broom measurement concept of the MPIR.

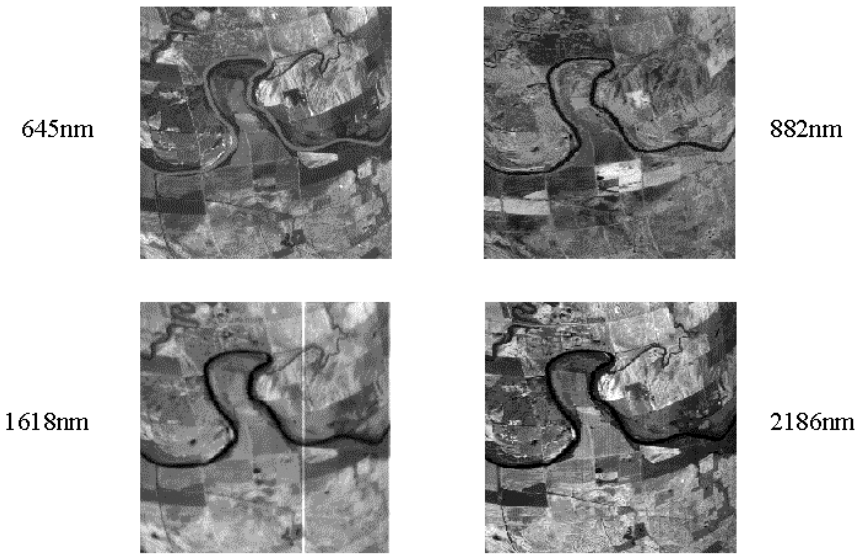

FIG. 7. Images obtained from four of the channels of the MPIR instrument recorded simultaneously. The push-broom data that produce the image represent an integration over 128-s interval on a clear day on 30 Sep 1996 and show the reflection from the surface over the Salt Fork of the Arkansas river in north central Oklahoma.

version of MPIR that flew on the Egrett. The version of the MPIR flown on subsequent campaigns included five modules: four from the previous S96 campaign plus one of the InSb modules (2.11–2.22 μm). The hardware for the other InSb and the three HgCdTe modules is near completion.

Figure 7 is an image derived from MPIR data for the four channels indicated. These images represent an integration of approximately 128 s of data obtained from the flight of 30 September 1996 and show the reflection from the surface over the Salt Fork of the Arkansas river in north central Oklahoma. For comparison purposes, all data in Fig. 7 are displayed as 256 × 256 element images even though channel 1 data are actually 512-element resolution. No channel 3 data are displayed since this channel lies in a strong water absorption band that produces very little signal under the clear-sky conditions encountered during this flight.

c. The UAV-CMR

The UAV-CMR was developed by the Microwave Remote Sensing Laboratory at the University of Massachusetts-Amherst (UMass). Operating at 95.04 GHz, this radar produces reflectivity and Doppler velocity profiles with a range resolution of 15 m (1000 range gates) and was designed to meet the power, size, and weight constraints imposed by the UAV platform. Previous airborne millimeter-wave cloud radars, such as that flown on the Otter deployments, consumed more than 1 KW of power, occupied 9 cubic feet and weighed 110 kg. In its current state (Fig. 8), the UAV-CMR system consumes 150 W, occupies 1.8 cubic feet, and weighs 40 kg. In the final phase, UAV-CMR will consume 110 W, occupy 1.5 cubic feet, and weigh 30 kg. The CMR is currently undergoing some modifications to enhance the sensitivity of the radar and will be integrated into the ARM–UAV payload in the near future.

Field tests were performed at UMass as well as in the Su99 campaign to evaluate the performance of the UAV-CMR and further tests are underway. The UMass Cloud Profiling Radar System (CPRS) provided coincident W-band reflectivity measurements when tested at the surface and the airborne cloud radar provided similar comparative data in the Su99

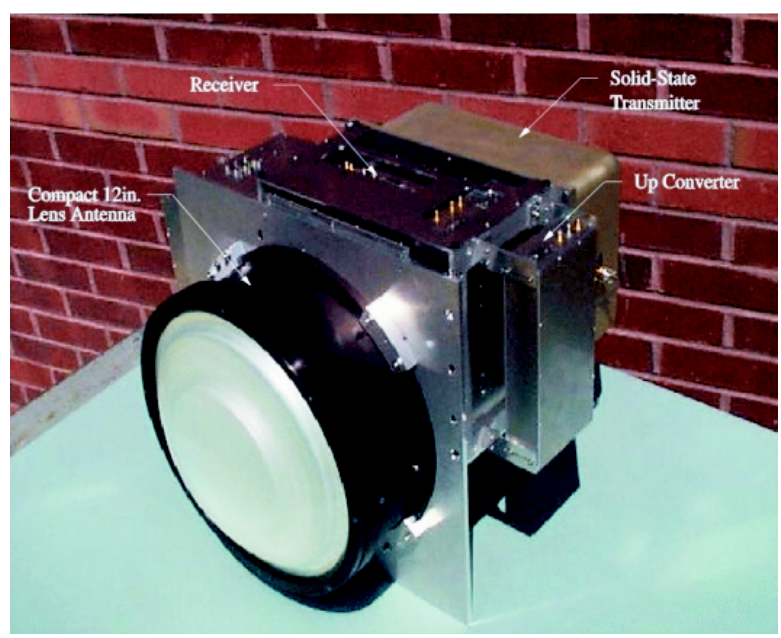

FIG. 8. The CMR system highlighting the compact nature of the radar.

campaign. Figure 9 shows one of the reflectivity images collected with the two systems operating on the ground. The data used to produce this image were obtained with the UAV-CMR configured with a 4-ft dish antenna that provided an additional 16 dB of sensitivity. The 12-in lens antenna shown in Fig. 8 was also used during these field tests and it performed as expected yielding a –20 dB sensitivity at 1 km. The UAV-CMR is currently being modified to increase the sensitivity of the radar.

d. Radiometric measurement comparisons

The examples of the data presented in Fig. 10 emphasize an important aspect of the measurement capabilities of the program, namely the degree of redundancy of the measurement capability that offers independent verification of the measurements and their estimated accuracies. Figures 10a and 10b show comparisons of spectral reflected solar fluxes simultaneously measured by the SSP and TDDR instruments of clouds during two flights of the F95 campaign. The fluxes correspond to narrow spectral bands centered at the wavelengths indicated. Similar comparisons of the SSP spectral radiance and the matched nadir radiance of the MPIR are compared for one of the flights of the F96 campaign in Fig. 10c. These measurements show a close degree of agreement indicating some confidence in the independent calibration methods applied to the individual sensors. The redundancy of measurements will continue to be an important feature of future measurements especially with the recent introduction of the SSFR to the payload.

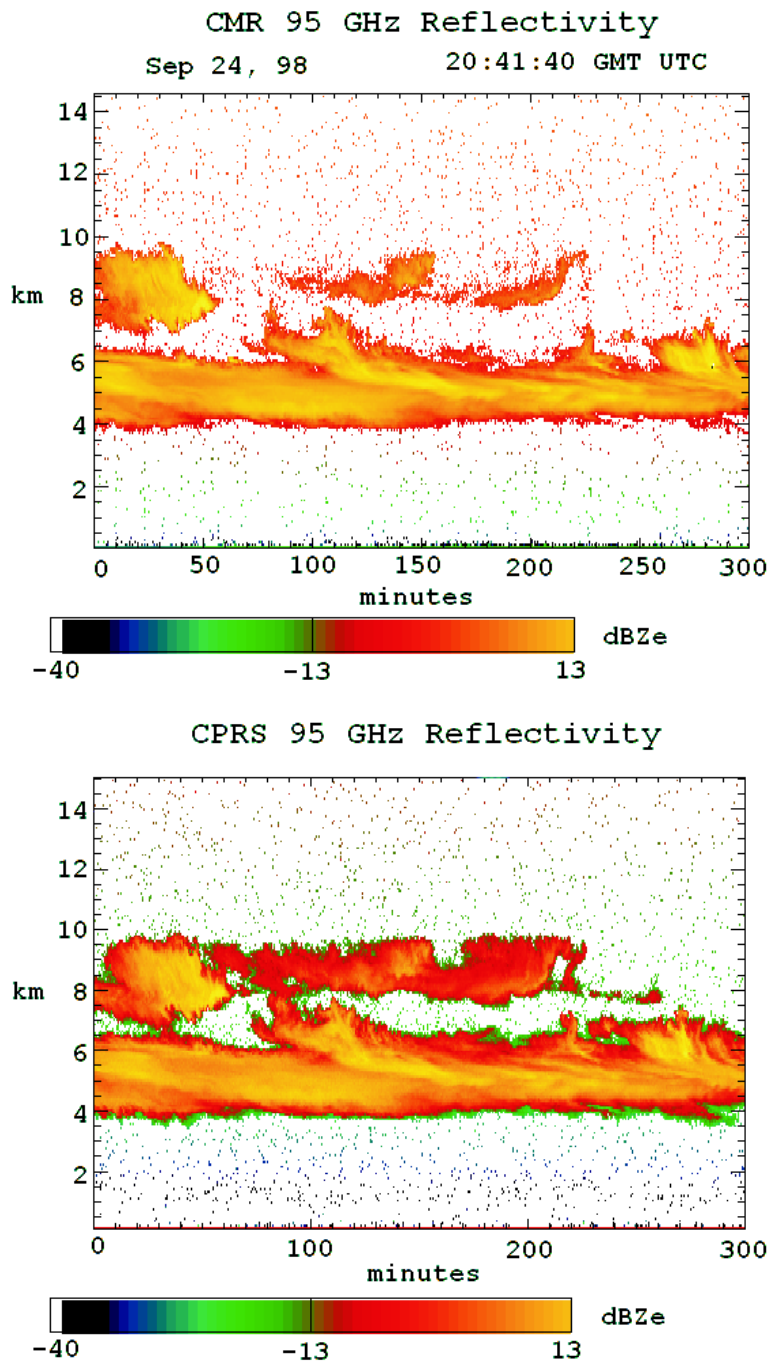

FIG. 9. Comparison of the CMR (upper) versus the CPRS (lower) measurements obtained with both radars located on the ground under a stratiform cloud observed at the University of Massachusetts.

5. Data systems and protocols

The ARM–UAV data are made widely available to the scientific community. Figure 11 is a schematic of the overall data management plan developed for the program and highlights the main steps in the flow of data from the sensor to the ultimate point of archive and thus the point at which the scientific community accesses the data. The basic elements of the data system are now described.

a. The telemetry system

A flexible telemetry system, both custom designed for ARM–UAV and based on commercial compo-

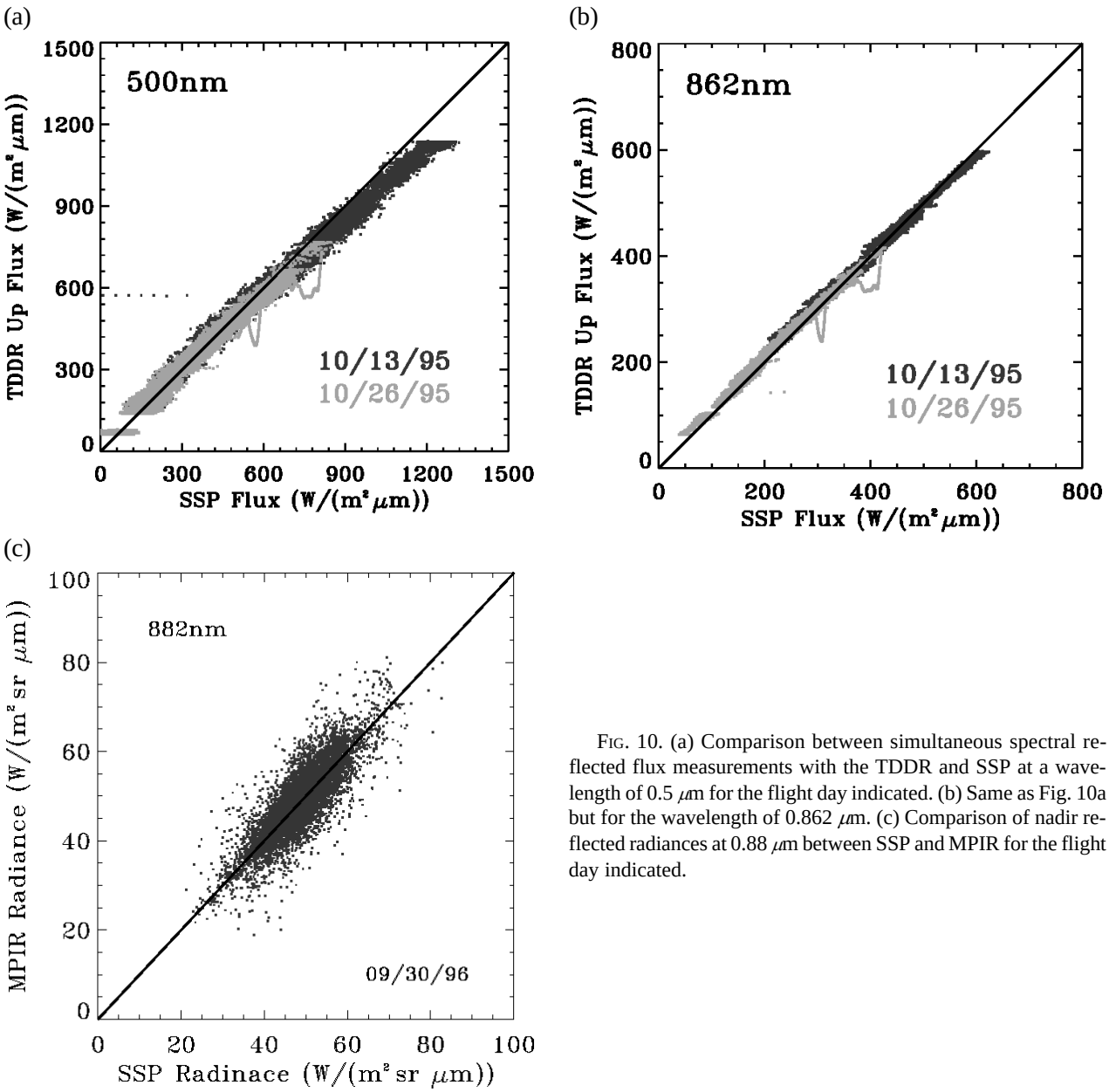

FIG. 10. (a) Comparison between simultaneous spectral reflected flux measurements with the TDDR and SSP at a wavelength of 0.5 μm for the flight day indicated. (b) Same as Fig. 10a but for the wavelength of 0.862 μm. (c) Comparison of nadir reflected radiances at 0.88 μm between SSP and MPIR for the flight day indicated.

nents, was developed for use on both the UAV and manned aircraft. The system can be expanded to include additional science instruments. It is capable of operation in an unpressurized aircraft at an altitude of 20 km with flight duration of 72 h. The telemetry system also allows the instrument mentor to monitor the instrument performance in flight and obtain real-time science data during flight with the advantage that the science mission and flight parameters may be modified while the UAV is airborne.

There are two main components of the telemetry system. The first is the aircraft component that collects multiple digital and analog streams from each instrument and transmits these data to a ground receiving station via a 4 W E-band transmitter operating at a frequency of either 2205.5 or 2235.5 MHz. The second component is the payload ground station that receives the data transmitted from the aircraft payload, distributes the data to various workstations, and provides uplink commands from the ground operations site to the aircraft. The payload ground station is configured as a recording and data processing facility receiving input from up to two automatic radio-frequency tracking antennae. Uplink commands to the UAV are originated on a laptop computer and routed to the UAV's control facility via an RS-422 serial stream. Important secondary capabilities of the ground station include 1) the display of real-time payload state of health in-

cluding selected diagnostic measurements, and 2) the dissemination of quick assessment science data to instrument mentors, as discussed below.

b. On-site data management system

An on-site data management system consisting of several computers linked to each other, the Payload Ground Station, and the Internet serves a number of important functions during the operation of the aircraft. The primary purposes of the system are to aid in mission and science planning and analysis as well as to monitor the status of the airborne instruments and payload. The system also accesses data from a number of sites such as the SGP Cloud and Radiation Testbed (CART) site when operating in that vicinity, as well as other data including meteorological and satellite data collected from various sources. A quick-look data capability that forwards data from all mission aircraft by the payload ground station in real time to the primary quick look computer in the science facility is also a capability developed as part of the system. In some cases, the quick-look data are subsampled to reduce the real-time computing load in the payload ground station. The primary quick-look computer prepares the data for display and distributes the data to the instrument mentor computers. It also provides displays for the mission scientist, mission controller, and technical support to aid in analysis of the scientific data, in aircraft flight coordination and control, and monitoring of the payload and instrument status. This capability coupled with the uplink allows the instrument mentor to alter the state of an instrument to either improve performance or safeguard the instrument against major malfunctions.

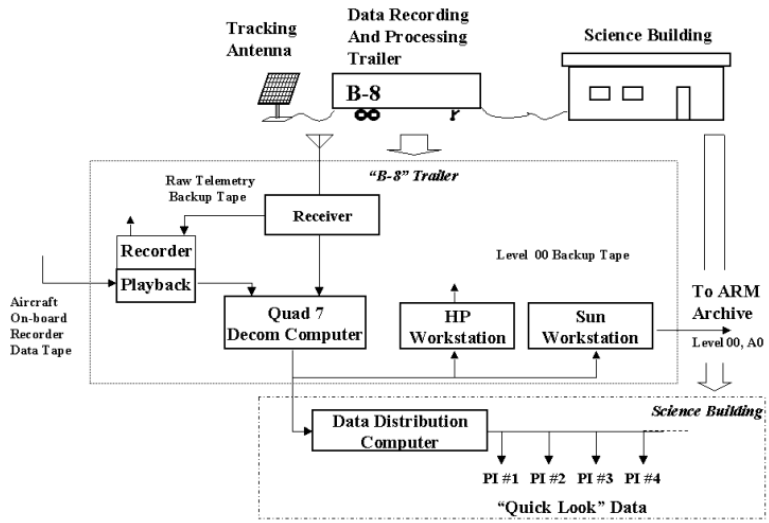

FIG. 11. The data system flow diagram.

c. Postflight data management, data reduction, and archive

Postflight data management converts all data collected from the onboard aircraft instruments to a complete, well-documented dataset of known and reasonable quality. The postflight processing system merges information from the three sources (data tapes, mission logs, and instrument lists) to produce the lowest level (a0) releasable data. During this processing, necessary documentation is added and various checks are performed. The level a0 data are distributed to the instrument mentors for additional value-added processing. The instrument mentors provide validation files and derived, higher-level (a1,b1) data that are collected by the primary processing facility. The data, written as netCDF data files, have considerable information about the data and limited information about the source instrument in the file header. The validation files contain more detailed information about the data, the source instrument, the processing algorithm, calibration factors, and quality check procedures.

In addition to the scientific data and validation files, the complete UAV mission dataset includes a number of files that document the flights both operationally and scientifically. Such documentation may include the mission experiment plan, a summary of each flight in a mission including the weather conditions and items of scientific note by the Mission Scientist, the full set of Mission Scientist and Mission Controller logs, flight cards, and README files with important notes specific to a mission, flight, aircraft, or instrument. A document explaining the directory structure and naming conventions is also provided. Ancillary data that are not normally archived by the ARM data system are collected, documented, and stored with the UAV program data. The dataset is transferred to the ARM Archive for access by the general scientific community when deemed complete.

6. Selected ARM–UAV science results

a. MPIR measurements for improving satellite algorithms

A number of different steps are required to convert uncalibrated narrowband radiances, such as radiances

obtained from various operational imagers, to calibrated narrowband fluxes and eventually broadband fluxes. Steps include vicarious calibration of the satellite image data and conversion of radiances to fluxes using bidirectional reflectance distribution funcions tions (BRDFs). BRDFs are distributions of reflection functions that are created as a function of the angle formed between the angle of solar incidence (solar zenith angle, SZA) and the view angle of the instrument (viewing zenith angle, VZA). Since BRDFs vary from scene to scene it is not possible to apply one single BRDF to the radiances measured over the diversity of scenes such as encountered within the field of view of any given satellite. The approach typically employed is to classify scenes and determine the BRDF appropriate to that scene. For example, the Earth Radiation Budget Experiment uses 12 different scenes and accordingly 12 different BRDFs (Wielicki and Green 1989) to determine the fluxes. The Clouds and the Earth's Radiation Energy System proposed an expanded classification in excess of 200 scenes (Wielicki et al. 1996).

Mayor et al. (1998) and Minnis et al. (2000, manuscript submitted to *J. Geophys. Res.*, hereafter MMKCDP) used the data collected from the MPIR during the F96 campaign both to test the calibration of channel 1 of the *GOES-8* imager and to derive a set of BRDFs for the scenes observed. The difficulty with measurement of the BRDF from conventional aircraft measurements is the compromised range of both SZA and VZA encountered. A particular advantage of the UAV in the development of the BRDFs is its ability to remain aloft over the same scene for extended periods covering a much wider range of SZAs than is possible with normal manned aircraft experiments.

MMKCDP composited MPIR channel-1 data obtained from three of the clear-sky flights from F96 (29 September, 3 October, and 4/5 October) to obtain clear-sky BRDFs. Data from these flights were taken at flight altitudes between 6 and 12 km and for VZAs ranging from 0° to 60°. Two of the flights occurred near noon (SZA~45°) and the 24-h flight covered the range of SZAs from 53° to 90°. These flight data were averaged into zenith and azimuth angle bins and then corrected from flight level to the top of the atmosphere following the methods of Minnis et al. (1993). Although the MPIR on the UAV views only to 40°, the 11° tilt of the instrument to port extends this range from 29° to 51° and further banks of the UAV increased the VZA to 60°. Figure 12a shows a set of the results for three SZAs. The combined flight paths yield complete coverage out to a 60° VZA for SZA < 70°. These results show the typical behavior for land surfaces, enhanced reflectance near the antisolar point (the so-called hot spot), and increasing forward scattering as SZA increases. The darker areas near the center left of each plot are the result of shadowing by the vegetation and surface structures. Bidirectional reflectance varies by more than a factor of 2 over the observed angles, even for the relatively flat terrain of the SGP area. Because these patterns vary with the terrain and vegetation and are so critical for radiation budget and remote sensing, it is clear that the measurements represented in Fig. 12a are needed for many different surface types and atmospheric conditions.

Although complete angular sampling could not be obtained from these particular measurements, the reflectances for many of the missing angles beyond 50° VZA and 50° SZA can be estimated by application of the Helmholtz Principle of Reciprocity. Testing of this principle showed that it produced rms errors of 15% for the areas viewed by MPIR during these flights. Use of the resulting reflectance estimates produced a complete pattern of hemispherical bidirectional reflectance for SZA 45° (Fig. 12b). However, because of a lack of measurements beyond VZA = 60°, no additional information could be derived for SZAs > 60° through the reciprocity approach. Other bin-filling techniques are required for those other angles. By increasing the tilt of the MPIR on future flights, it will be possible to obtain almost complete hemispherical coverage of bidirectional reflectance at all VZAs. The range of SZAs is limited only by the time of year and latitude of the flights because the UAV can remain on station repeating the flight pattern as often as needed to account for surface and atmospheric variations.

b. Remote sensing of cloud optical properties

The ARM–UAV sensor payload has evolved into a powerful observing system for several cloud remote sensing applications. Combining multispectral radiometer observations such as the spectral radiance measurements provided by the SSP or MPIR with the high vertical resolution cloud altimetry (e.g., from the CDL or the cloud radar) enables a more capable retrieval of cloud optical depth and effective particle radius.

A forward model and inversion algorithm described by Miller et al. (2000, hereafter MDSHP) has been applied to simulate the measurements of the SSP as a way of illustrating the utility of the ARM–UAV multisensor platform in the retrieval of cloud optical properties. The model incorporates information both

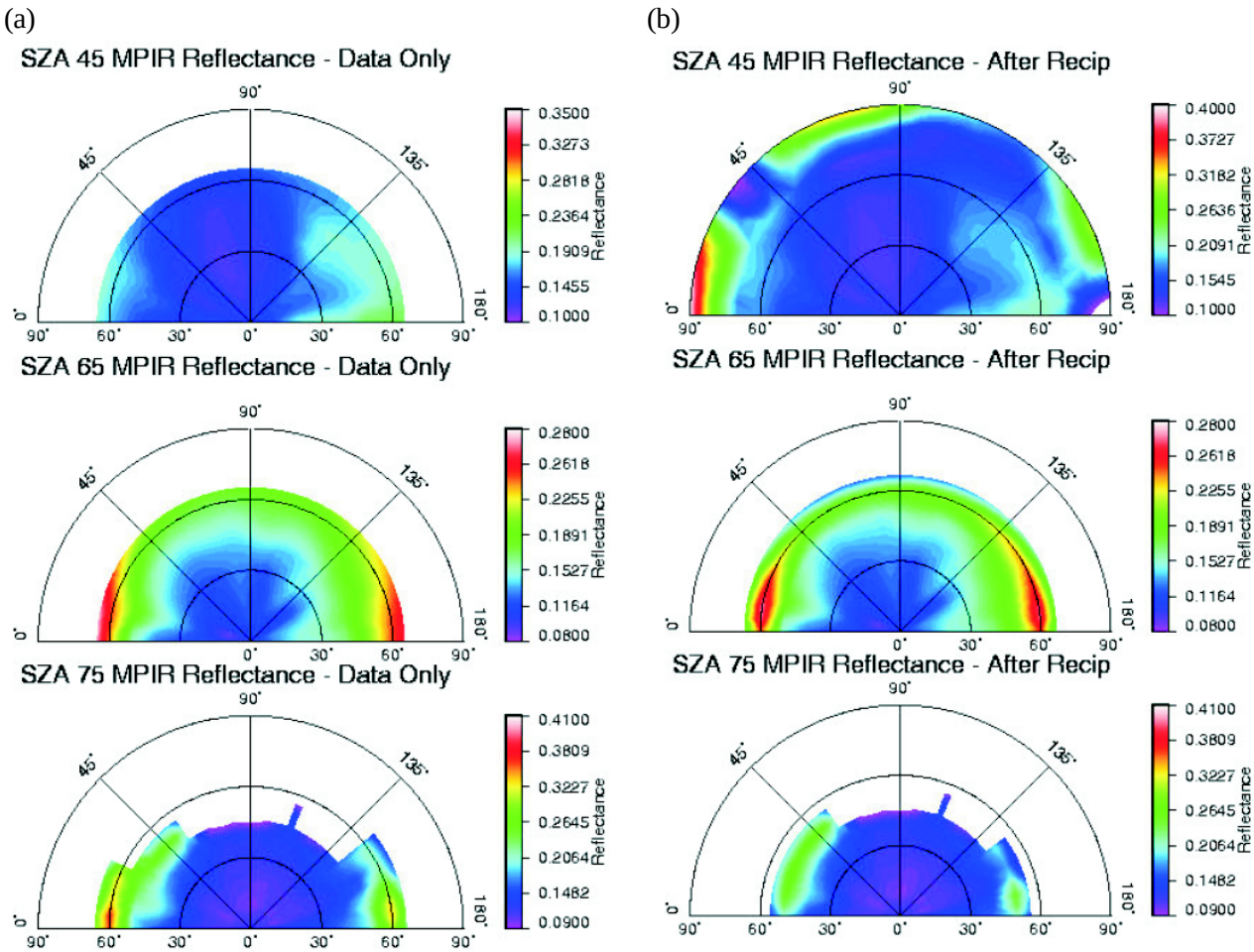

FIG. 12. (a) The MPIR derived BRDF determined from measurements made at the time of day corresponding to three SZA values stated. (b) As in (a) but with reflectances deduced at VZAs greater than 60° under the assumption of reciprocity and other filling methods applied to measurements collected with the setting and rising of the sun during the 24-h flight of 5/6 Oct flight as part of F97.

from SSP spectral radiances and CDL-derived cloud profiles into an iterative optimal estimation algorithm of the form developed by Rodgers (1976) and Marks and Rodgers (1993). In addition to providing useful diagnostic parameters describing retrieval performance (e.g., the reliance of the convergent solution on a priori assumptions), the algorithm provides a means of quantifying the error in terms of forward model (e.g., assumptions about scattering phase function, temperature/gas/aerosol profile, etc.), and measurement uncertainty components together.

An example of optical depth retrievals obtained using data collected during the S95 campaign (ARESE) and applied to the retrieval algorithm described above is shown in Fig. 13 and other examples are discussed further in relation to the results presented below. For the particular case relevant to Fig. 13, the cirrus layer was located between about 8 and 10 km. The radiances measured by the nadir-oriented airborne SSP were used together with CDL cloud heights to retrieve cloud optical depth. Surface/lower-atmospheric aerosol albedos were computed from SSP-observed clear-sky scenes. Because the spectral range of this first-generation SSP instrument did not include wavelengths longer than 1.1 μm, retrieval of particle size was not available for this case. Those regions where the CDL does not penetrate the cloud completely (i.e., where surface returns are not observed) correspond to the highest observed SSP radiances and retrieved optical depths.

c. Evaluating cloud parameterizations within cloud-resolving and numerical weather prediction models

The cloud microphysical and radiative properties that can be derived from the suite of UAV measurements represent a valuable source of information for evaluating the way certain cloud processes are param-

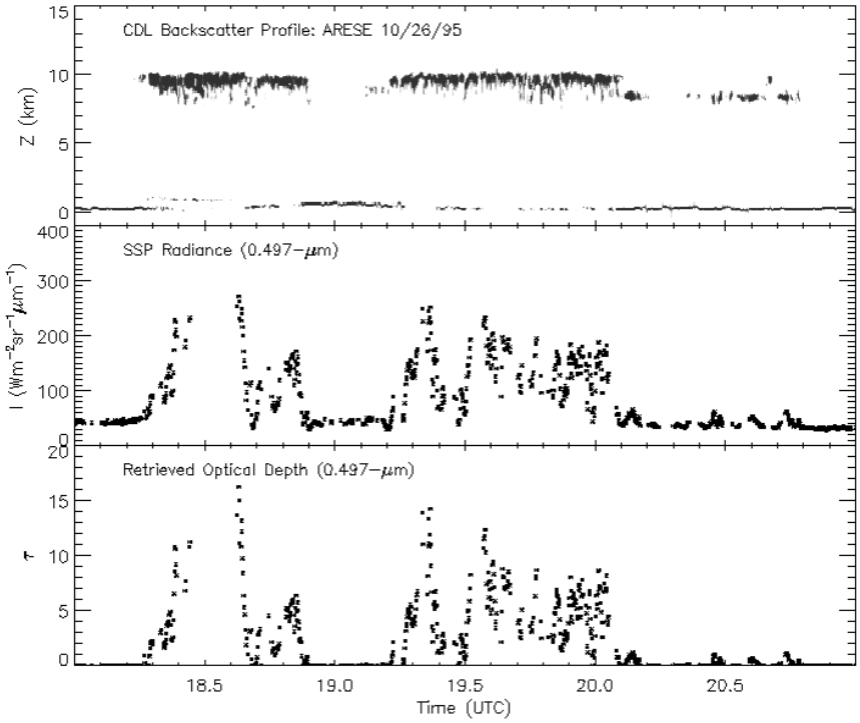

FIG. 13. An example of optical depth retrievals of a cirrus cloud layer between 8 and 10 km using data collected during the S95 campaign. The CDL backscattering cross section is shown in the upper panel and the SSP derived optical depths are indicated in the lower panel. Those regions where the CDL suffers total attenuation (i.e., where surface returns are not observed) correspond to the largest retrieved optical depths.

eterized in both cloud-resolving and weather prediction models. An example of this particular application using the data obtained from the S99 campaign is now described. The example presented corresponds to the case of a single layer of cirrus cloud observed on 30 April 1999. The data were obtained from sensors flown on the Altus II flown above the cirrus layer and the Twin Otter flown below in formation with the UAV. The data are compared to simulated observations derived from cloud data predicted by both a cloud-resolving model and the forecast model of the European Centre for Medium-range Weather Forecasts (ECMWF).

Figure 14 is the visible image obtained from *GOES-10* that provides the large-scale context for these measurements. An extensive layer of thin cirrus developed as part of the outflow of deep convection associated with an upper-level trough located west of the observing region. The portion of the layer of cirrus observed is indicated by the flight tracks of both the Altus II and the Twin Otter. Figure 15 presents the vertical cross section of the radar reflectivity obtained from the zenith pointed 94-GHz radar flown on the Twin Otter during this campaign (Fig. 15a) and the matching vertical cross section of lidar backscatter obtained from the nadir-pointed CDL on the Altus II. Also indicated are the portions of the time series that represent collocation of the two measurements. The lidar/radar measurements indicate a relatively deep layer of cirrus between approximately 10 and 14 km especially after 2300 h UTC. The optical depths retrieved from both SSP and GOES image data suggests that the cloud varied in its optical thickness up to a maximum of about 4 over the thickest portions of the cloud during the period from 2300 to 2400 UTC (Fig. 16).

Portions of the flight level data shown in Fig. 15 are reproduced in Fig. 16 along with the radar reflec-

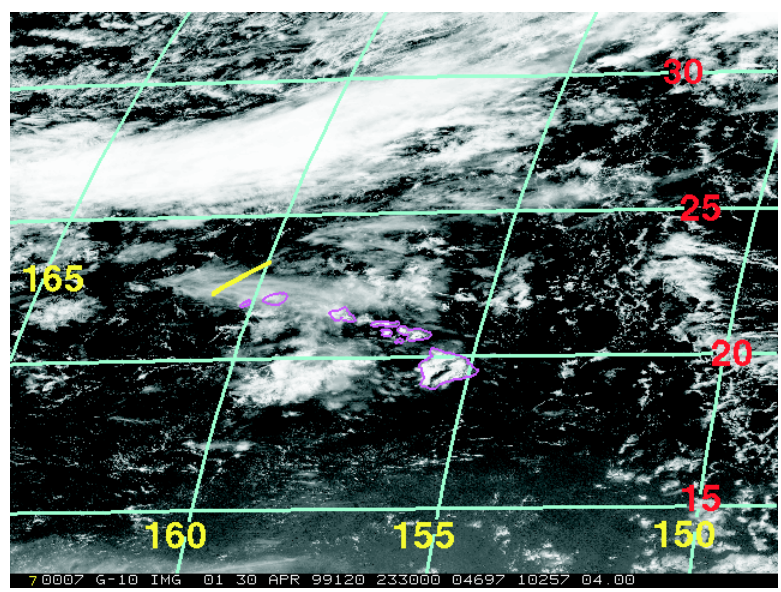

FIG. 14. GOES image for 30 Apr 1999 at 2330 UTC. Also shown are flight tracks of the aircraft.

tivity and lidar backscatter cross sections simulated from the ice water content obtained from time integrations of a two-dimensional cloud-resolving model. The radar reflectivity–ice water content relation to Sassen and Liao (1994) along with the ice water content–extinction and extinction to backscatter relations of Platt (1997) were employed to convert the model ice water contents to equivalent radar and lidar measured quantities. The cloud-resolving model used to simulate the cirrus ice-water content has full dynamics, radiation, and bulk microphysics and its heritage is the RAMS (Walko et al. 1996). The model was forced with the environmental profiles of temperature, moisture, and horizontal winds obtained from the 24-h forecast provided by the ECMWF. The details of these simulations and comparisons with other cirrus observed during the S99 campaign is a topic of another study. Also shown in Fig. 16e are the along-track optical depths of the cirrus derived from both the SSP radiances and matched *GOES-10* imager radiances in the retrieval scheme described by MDSHP plotted as a function of the measured radar reflectivity averaged through the vertical extent of the cloud.

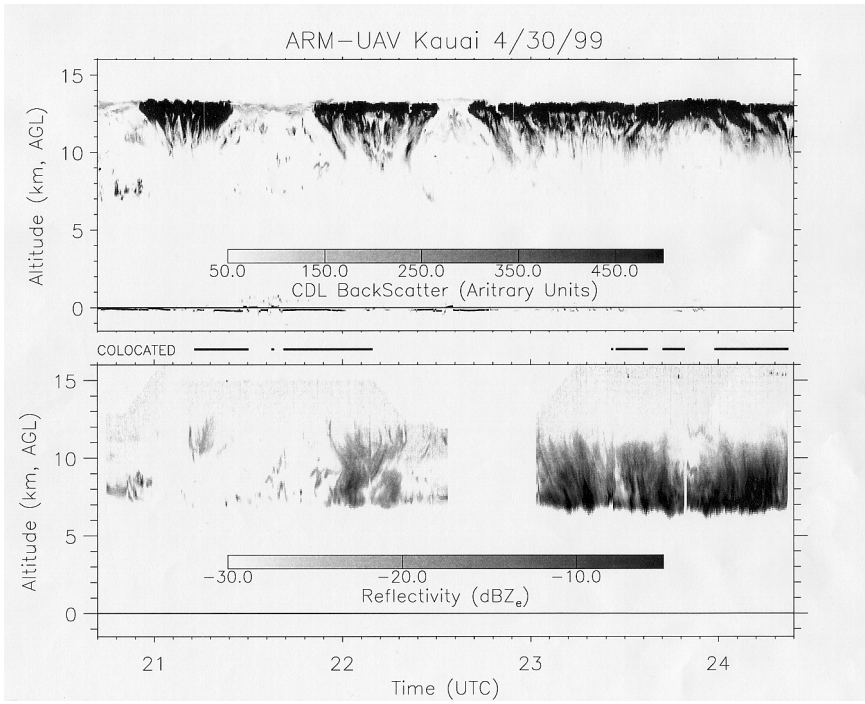

FIG. 15. Time–height cross sections of the CDL backscatter and the mm cloud radar reflectivity obtained from level flight legs above and below a cirrus cloud layer observed on 30 Apr 1999. The times when the lidar and radar were deemed to be collocated are also indicated.

It is not expected that the model simulations of the cloud variability should match the observations in any real quantitative detail. There are a number of reasons why the mesoscale structure of the predicted cloud differs from the observed cloud. The forcing applied in the model is homogeneous and lacks any mesoscale structure, the model cloud is two-dimensional, and the model cross section shown is not directly comparable to the measured cross section obtained from the aircraft data. Perhaps more appropriate is the comparison of the statistics of the model fields compared to similar statistics of the observations as given in Fig. 17 that presents the vertical profiles of the measured radar reflectivity averaged along the flight track of the Twin Otter over the period of time from 23.11 to 23.89 UTC (refer to Fig. 15 for reference). These measured profiles are subsequently compared to the equivalent domain averaged reflectivity and backscatter profiles derived from the cloud ice water contents as well as the simulated observations derived from the ECMWF 24-h forecast ice water content field. The comparisons reveal a remarkable degree of similarity between the radar reflectivity profile predicted by both models with the profiles measured by the Airborne Cloud Radar and CDL. This agreement implies some degree of realism of the modeled ice water contents although the latter were not measured. This implication is further supported by the broad agreement between the optical depth distributions derived from both the retrieved optical depths and the optical depth distributions calculated from the model ice water contents (Fig. 18).

7. Summary

The U.S. DOE ARM program has established a UAV-based measurement program that has clearly demonstrated how measurements from unmanned aircraft platforms operating under the various constraints imposed by different science experiments can contribute to our understanding of cloud and

radiative processes. The various phases of the program's development and the subsequent achievements of the program are discussed in the paper. The achievements of the program have occurred as a consequence of a goal-oriented phased approach to the program's development resulting a series of measurement campaigns (eight) that yielded a number of the significant highlights including the following.

1) The first atmospheric science measurements from unmanned aircraft, including the first profiles of radiative fluxes from a UAV, the first unescorted flight of a UAV in class A airspace, the first science measurements from a UAV operated on a station continuously for more than 24 h and the first science measurements from a UAV above 16 km. The UAV platforms deployed under the auspices of the program are the Gnat-750, the Altus, and Altus-II UAVs provided by General Atomics Aeronautical Systems, Inc.
2) The development of a versatile and powerful payload capability that includes active systems such as millimeter-wave radar and lidar as well as passive spectrometer and radiometer systems.
3) The development of a mature data system that provides direct real-time downlink of the data to the instrument mentor during flight and an archive that provides access of the data by the general science community.
4) The development of aircraft operational systems that allow for the formation flying of multiple aircraft thus enabling close coordination of cloud observations from two (or more) aircraft.

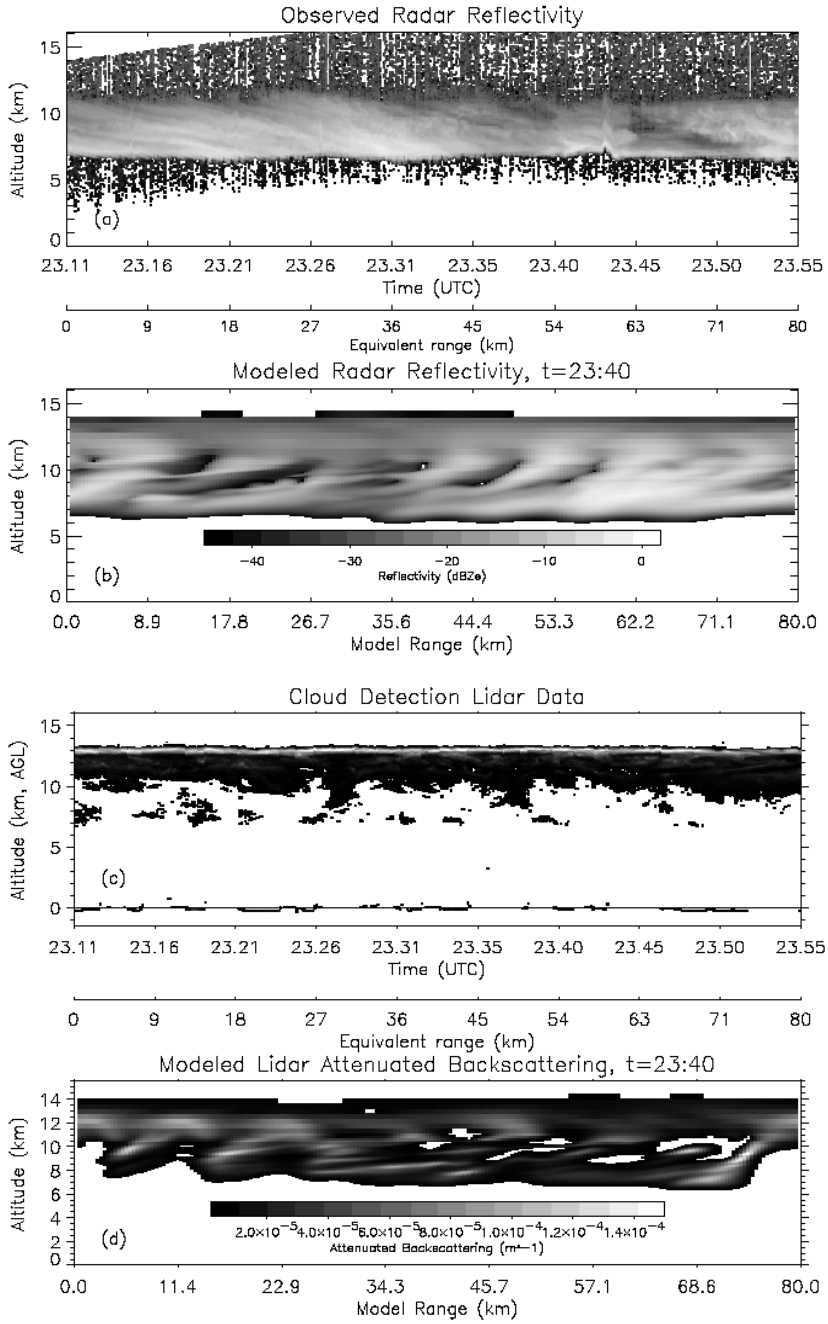

FIG. 16. (a) The height cross sections of radar reflectivity obtained from the ACR on the Twin Otter; (b) CRM-derived radar reflectivity cross sections; (c) as in (a) but for CDL; and (d) as in (b) but for CRM.

The program evolved through four different phases of activity each culminating in one or more flight campaigns. A total of eight flight campaigns with over 140 h of science flights using a UAV have been carried out at this time. The goals of three of the four phases have been achieved and activities under phase IV are continuing. Selected examples of the data obtained from various campaigns highlight the power-

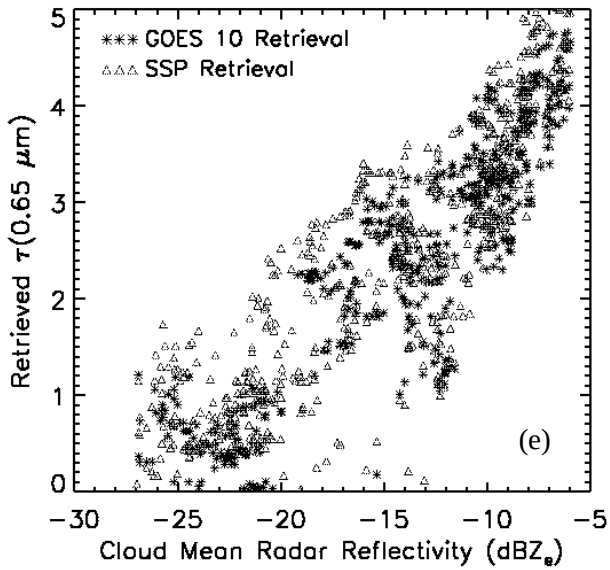

FIG. 16. (e) SSP and GOES optical depths contrasted against the measured radar reflectivity.

ful nature of the observing system developed under the auspices of the ARM–UAV program. The examples described in section 6 emphasize the value of the measurements for several applications involving the study of radiative transfer through clouds, the evaluation of cloud parameterizations, the vicarious calibration of satellite sensors, and the development and evaluation of cloud remote sensing methods.

Acknowledgments. The authors would like to acknowledge the Department of Energy's Atmospheric Research Measurement–Unmanned Aerospace Vehicle (ARM–UAV) progam and the Department of Defense's Strategic Environmental Research and Development Program (SERDP) for sponsoring much of the work described in this article. The S99 and Su99 campaigns were also supported under NASA Grants NAG-961158 and 1212032 as part of the radiation program of NASA Earth Science Enterprise. We also acknowledge the contributions of Anton Beljaars of the ECMWF in providing the cirrus cloud forecasts used in analyses of S99 data.

Appendix: The Los Alamos National Laboratory (LANL) Radiometric Calibration Facility

The ARM–UAV program reflects the ARM emphasis on measurement accuracy and the program management decided that all calibrations should be referenced to the same National Institute of Standards and Technology (NIST)–traceable standards, and targeted challenging accuracies for the radiometric calibrations. Appropriate equipment and infrastructure were established at LANL and the calibration activities were linked to NIST, the National Oceanic and Atmospheric Administration (NOAA), and others to tie the calibrations to national and international standards.

The Los Alamos radiometric calibration laboratory is a 4000 sq. ft facility equipped with state-of-the-art NIST-traceable optical and infrared radiation sources and radiometers, along with IR-Visible-UV spectrometers, and HeNe, GreenNe, and CO_2 lasers. It can provide for the complete calibrations of instruments in the spectral range 0.5–12 μm in both the radiometric and spectral domains; broadband calibrations extend well beyond this range including into the UV portion of the spectrum.

Calibrated detectors include 1) a Cambridge Research cryogenic cavity electrical substitution radiometer with absolute accuracy of 0.02%–0.05% (1σ) and spectrally flat response from 0.25 to 40 μm, 2) two Eppley absolute cavity electrical substitution radiometers, designed to measure direct normal-incidence solar radiation at the 0.1% (1σ) accuracy level. These two instruments were recently tied to the World Radiometric Reference through their participation in an ARM-sponsored intercomparison with 17 other absolute cavity radiometers, 3) a NIST-designed and calibrated Si composite bolometer, with spectral calibration from 2 to 15 μm to an accuracy of 1.4%, 4) silicon trap photodiodes with NIST spectral radio-

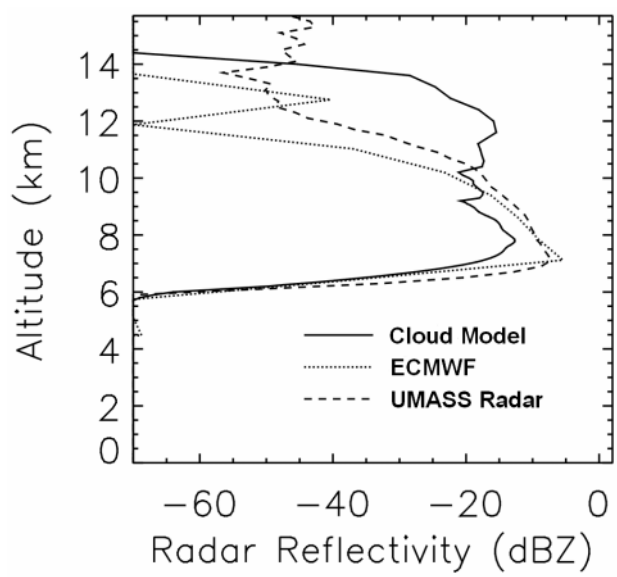

FIG. 17. (a) The profiles of radar reflectivity averaged across the domain of the CRM and along the flight track of the Otter. The ECMWF profile corresponds to the 24-h forecast field of the grid point of the model that is the closest match to the flight data.

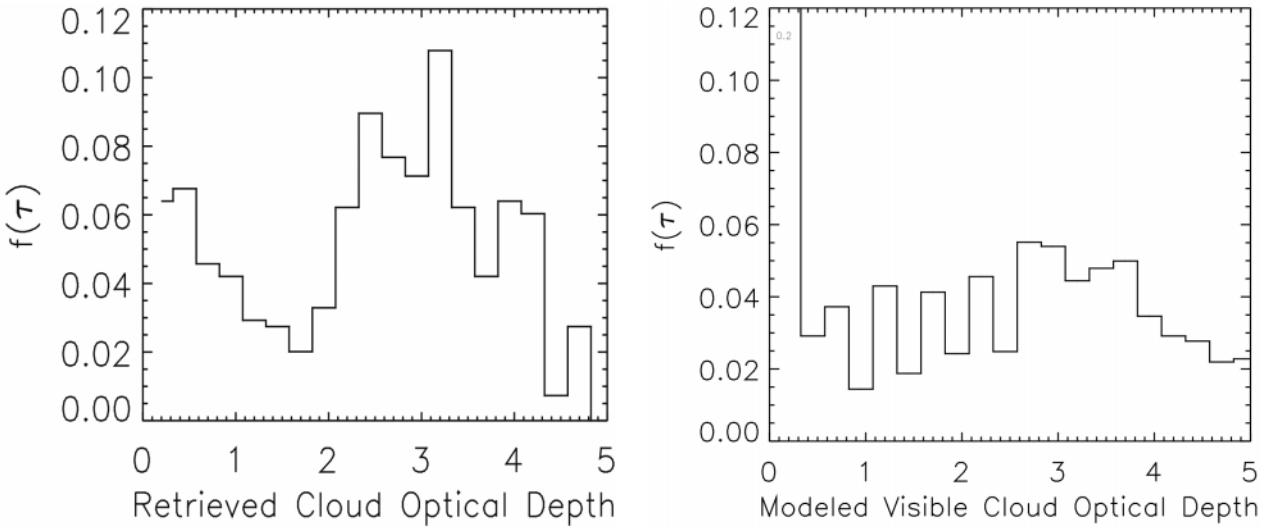

FIG. 18. Optical depth probability distribution functions (pdf) derived from the retrieved optical depths obtained from the SSP on the Altus vs. pdf derived from CRM simulations.

metric response calibration better than 1% (3σ) over the 0.35–1.1-μm range and 0.33% (3σ) in the 0.4–0.9-μ range, and 5) commercial (Laser Precision) pyroelectric radiometers. In addition, several other high quality IR detectors are in the calibration laboratory's inventory. Also available are calibrated InSb and HgCdTe infrared cameras.

This calibration facility has participated in a number of activities, including those listed below.

Cavity Radiometer Intercomparison: Eighteen electrical substitution absolute cavity radiometers simultaneously measured the direct-beam solar irradiance from the same location, over a period of several days in October 1994. This work tied the calibration of each of the participating radiometers to both the ARM program CART site reference set, and (through the participation of the NREL–NOAA reference radiometers, recently returned from the World Radiometric Intercomparison in Davos, Switzerland) to the World Radiometric Reference. Absolute calibration of the radiometers is now known to within 0.1%, with respect to the World Radiometric Reference.

Pyrgeometer Round-Robin: Six Eppley pyrgeometers were calibrated by a variety of methods at twelve standards laboratories around the world, including LANL, NREL, NOAA, the Eppley Laboratory, the World Radiation Center in Switzerland, and national meteorological and standards laboratories in Canada, Australia, the United Kingdom, Germany, and Japan. The aim was to establish the validity and degree of equivalence of the various calibration strategies used for these ubiquitous instruments. Calibration at Los Alamos utilized our NIST fluid-bath blackbody operating at a variety of temperatures from 5° up to 70°C. A method of radiatively heating and cooling the filter dome of these instruments was developed, allowing calibration of the dome emission contribution to the pyrgeometer output. Using this method, it was found that dome emission effects can contribute very substantially to the pyrgeometer output—as much as 20 W m^{-2} K^{-1} of temperature difference between the filter dome and reference junction—thus underlining the need for thorough calibration of dome effects for all such instruments. Current plans include return of the pyrgeometers to Los Alamos for spectral characterization of the filter domes.

SSP calibration: Multiple calibrations of SSP were performed at Los Alamos over the course of the ARM–UAV program as described by Stephens et al. (1999). Calibration tasks performed included: 1) characterizing, at multiple wavelengths, the quality of polarization and the polarization orthogonality of the two linear polarization channels; 2) complete mapping at 1-nm resolution of the relative spectral responsivity at each of the 107 encoded positions along SSP's circularly variable filter for each of SSP's four channels (two linearly polarized narrow field of view channels, unpolarized narrow field-of-view channel, unpolarized quasi-hemispherical flux channel); 3) absolute spectral response calibration at each wavelength for each of the four channels; 4) angular response calibration of the quasi-hemispherical flux channel at each wavelength; 5) calibration of the temperature dependence

of the absolute spectral response. This involved construction of a custom variable-temperature environmental chamber for SSP, capable of temperatures as low as –80°C.

MPIR calibration: First Los Alamos calibration activity with MPIR was ground support during the spring 1996 campaign. Upon delivery to Los Alamos, characterization of the four shortest wavelength MPIR channels revealed a latency/readout-rate mismatch in the near-IR arrays, leading to context-dependent nonlinear behavior, and a temperature-related responsivity drift in the Si cameras. Nevertheless, spectral characterization of all four channels was performed, within the nonlinear and drift limitations, and an absolute calibration and spatial flat fielding of the Si cameras was performed.

References

Albritton, D. L., F. C. Fehsenfeld, and A. F. Tuck, 1991: Instrumental requirements for global chemistry. *Science,* **250,** 75–81.

Bluth, R. T., P. A. Durkee, J. H. Seinfield, R. C. Flagan, L. M. Russell, P. A. Crowley, and P. Finn, 1996: Center for Interdisciplinary Remotely-Piloted aircraft studies (CIRPAS). *Bull. Amer. Meteor. Soc.,* **77,** 2691–2699.

Holland, G. J., T. McGeer, and H. Youngren, 1992: Autonomous aerosondes for economical atmospheric soundings anywhere on the globe. *Bull. Amer. Meteor. Soc.,* **73,** 1987–1998.

King, M. D., Y. J. Kaufman, W. P. Menzel, and D. Tanré, 1992: Remote sensing of cloud, aerosol and water vapor propreties from the moderate resolution imaging spectrometer (MODIS). *IEEE Trans. Geosci. Remote Sens.,* **30,** 2–26.

Langford, J. S., 1990: New aircraft platforms for Earth system science: An opportunity for the 1990s. *Proc. 17th Congress Int. Council of the Aeronautical Sciences,* Stockholm, Sweden, ICAS90 5.8.1.

Li, Z., A. P. Trishchenko, H. W. Barker, G. L. Stephens, and P. Partain, 1999: Analyses of Atmospheric Radiation Measurement (ARM) programs Enhanced Shortwave Experiment (ARESE) multiple data sets for studying cloud absorption. *J. Geophys. Res.,* **104,** 19 127–19 134.

Marks, C. J., and C. D. Rodgers, 1993: A retrieval method for atmospheric composition from limb emission measurements. *J. Geophys. Res.,* **98** (D8), 14 939–14 953.

Marshak, A., A. Davis, W. Wiscombe, and R. Cahalan, 1997: Inhomogeneity effects of cloud shortwave absorption measurements: Two aircraft simulations. *J. Geophys. Res.,* **102,** 16 619–16 637.

Mayor, S. D., P. Minnis, and G. S. Phipps, 1998: Clear-sky bidirectional reflectance functions derived from ARM-UAV MPIR Data over the ARM Southern Great Plains Site. *Proc. Eighth Annual Atmospheric Radiation Measurement (ARM) Science Team Meeting,* Tucson, AZ, ARM, 461–465.

Miller, S. D., C. K. Drummond, G. L. Stephens, A. K. Heidinger, and P. T. Partain, 2000: A multisensor-satellite diagnostic cloud property retrieval scheme. *J. Geophys. Res.,* **105,** 19 955–19 971.

Minnis, P., K. Liou, and Y. Takano, 1993: Inference of cirrus cloud properties using satellite-observed visible and infrared radiances. Parameterization of radiance fields. *J. Atmos. Sci.,* **50,** 1279–1304.

——, S. Mayor, M. M. Khaiyer, D. R. Cahoon, D. R. Doelling, and G. S. Phipps, 2000: Clear-sky bidirectional reflectance functions derived from ARM-UAV MPIR and CERES helicopter data over the ARM southern Great Plains site. *J. Geophys. Res.,* in press.

Pilewskie, P., A. F. H. Goetz, D. A. Beal, R. W. Bergstrom, and P. Mariani, 1998: Observations of the spectral distribution of solar irradiance at the ground during SUCCESS. *Geophys. Res. Lett.,* **25,** 1141–1144.

Platt, C. M. R., 1997: A parameterization of the visible extinction coefficient of ice clouds in terms of ice/water content. *J. Atmos. Sci.,* **54,** 2083–2098.

Rodgers, C. D., 1976: Retrieval of atmospheric temperature and composition from remote measurements of thermal radiation. *Rev. Geophys. Space Phys.,* **14,** 609–624.

Sadowy, G. A., and Coauthors, 1997: The NASA DC-8 airborne cloud radar: Design and preliminary results. *Proc. Int. Geoscience and Remote Sensing Symp.,* Singapore, Geoscience and Remote Sensing Society.

Sassen, K., and L. Liao, 1994: Investigation of relationships between Ka-band radar reflectivity and ice and liquid water contents. *Atmos. Res.,* **34,** 231–248.

Stephens, G. L., R. F. McCoy Jr., R. B. McCoy, P. Gabriel, P. Partain, S. D. Miller, and S. Love, 2000: A multipurpose scanning spectral polarimeter (SSP): Instrument description and sample results. *J. Atmos. Oceanic Technol.,* **17,** 616–627.

Stokes, G., and S. Schwatrz, 1994: The atmospheric radiation measurement (ARM) program: Programmatic background and design of the cloud and radiation test bed. *Bull. Amer. Meteor. Soc.,* **75,** 1201–1221.

Toon, O. B., and R. C. Miake-Lye, 1998: Subsonic aircraft: Contrail and cloud effects special study (SUCCESS). *Geophys. Res. Lett.,* **25,** 1109–1112.

Valero, P. J., W. J. Gore, and L. P. Giver, 1982: Radiative flux measurements in the troposphere. *Appl. Opt.,* **21,** 831–838.

——, S. K. Pope, R. G. Ellingson, A. W. Strawa, and J. Vitko Jr., 1996: Determination of clear-sky radiative flux profiles, heating rates, and optical depths using unmanned aerospace vehicles as a platform. *J. Atmos. Oceanic Technol.,* **13,** 1024–1030.

——, A. Bucholtz, B. C. Bush, S. K. Pope, W. D. Collins, P. Flatau, A. Strawa, and W. J. Gore, 1997: Atmospheric Radiation Measurement Enhanced Shortwave Absorption Experiment (ARESE): Experiment and data details. *J. Geophys. Res.,* **102,** 29 929–29 937.

Walko, R. L., W. R. Cotton, M. P. Meyers, J. Y. Harrington, 1996: New RAMS cloud microphysics parameterization. Part I: The single-moment scheme. *Atmos. Res.,* **38,** 29–62.

Wielicki, B., and R. N. Green, 1989: Cloud identification for ERBE radiative flux retrieval. *J. Appl. Meteor.,* **28,** 113–1146.

——, B. R. Barkstrom, E. F. Harrison, R. B. Lee III, G. L. Smith, and J. E. Cooper, 1996: Clouds and the Earth's Radiant Energy System (CERES): An Earth Observing System Experiment. *Bull. Amer. Meteor. Soc.,* **77,** 853–868.

ACCESS TO THE **ENTIRE** AMS JOURNAL ARCHIVES IS HERE!

Currently, AMS Journals Online cover the period from 1997 to the present. In response to requests by the community to extend access to include years prior to 1997, and in an effort to allow scientists and students to efficiently gain access to a broader and more historical perspective on their current research, the Society is pleased to offer the AMS Legacy Journals Online. For a fixed, one-time price, subscribers may purchase *perpetual online access to every article published prior to 1997 in any or all of our journals* (back to 1974 for *Monthly Weather Review).* Search capability at the title, author, abstract, and full-text levels makes the Legacy an incredibly powerful and exciting research tool. The table below shows the number of years of back issues that will be available for each issue.

Journal Title	Years in Back Files
Journal of the Atmospheric Sciences	54
Journal of Applied Meteorology	35
Journal of Physical Oceanography	26
Monthly Weather Review (AMS years only)	23
Journal of Atmospheric and Oceanic Technology	13
Weather and Forecasting	11
Journal of Climate	9

For ordering information for AMS Legacy Journals Online, see the AMS Web site for details. Please direct all other inquiries to the American Meteorological Society by e-mail at amssubs@ametsoc.org or by telephone at 617-227-2425.